

NT DEVELOPMENTS IN  
TROPHYSICS

---

---

ASTRONOMICAL SOCIETY OF THE PACIFIC  
CONFERENCE SERIES

U-262N #105  
979



Volume 12

THE EVOLUTION OF THE INTERSTELLAR MEDIUM

Edited by

Leo Blitz

## TURBULENT STRIPPING OF INTERSTELLAR CLOUDS BY INTERACTION WITH SUPERNOVA REMNANTS

Richard I. Klein

University of California, Lawrence Livermore National Laboratory and  
Department of Astronomy, University of California at Berkeley

Christopher F. McKee

Departments of Physics and Astronomy, University of California at Berkeley

Philip Colella

University of California, Lawrence Livermore National Laboratory and  
Department of Mechanical Engineering, University of California at Berkeley

### ABSTRACT

We present results for the interaction of a supernova remnant blast wave with a small interstellar cloud, using for the first time high resolution local adaptive mesh refinement techniques with an underlying second order accurate 2-D Godunov hydrodynamic scheme. The cloud shock is assumed to be strong enough that it is non-radiative. We follow the morphological evolution of the cloud in great detail as it undergoes a series of complex shock-shock interactions and Kelvin-Helmholtz and Rayleigh-Taylor instabilities. We demonstrate, over a large range of cloud densities and shock strengths, that clouds are efficiently destroyed in a few cloud crushing times (essentially, the Rayleigh Taylor time) by a combination of instabilities and large scale shear flow. We investigate the scaling properties of clouds of different densities and shocks of different strengths. Our results have uncovered the development of copious supersonic vortex rings produced in the shear flow layer of the interaction. These vortex rings may wrap up ambient magnetic fields, enhancing the synchrotron emission and possibly explaining the compact radio hot spots seen in Cas A. Our calculations have, for the first time, carried the cloud-shock interaction well into the fragmentation regime. We demonstrate that similar calculations with standard fixed grid hydrodynamic schemes would require one to two orders of magnitude more computational time than is needed with our adaptive mesh approach to achieve comparable results.

## INTRODUCTION

The interaction between supernova remnants (SNRs) and interstellar clouds in the galaxy is known to play a major role in determining the structure of the interstellar medium (ISM). We know that the ISM is highly inhomogeneous, consisting of both diffuse atomic clouds ( $T \sim 100\text{K}$ ) and dense molecular clouds ( $T \sim 10\text{K}$ ) surrounded by a low density warm ionized gas ( $T \sim 10^4\text{K}$ ) and by a very hot coronal gas ( $T \sim 10^6\text{K}$ ). Next to radiation directly from stars, supernova explosions represent the most important form of energy injection into the ISM; they determine the velocity of interstellar clouds, accelerate cosmic rays, and can compress clouds to gravitational instability, possibly spawning a new generation of star formation. The shock waves from supernova remnants can compress, accelerate, disrupt and render hydrodynamically unstable interstellar clouds, thereby ejecting mass back into the intercloud medium. Thus, while the interaction of the SNR blast wave with cloud inhomogeneities can clearly alter the appearance of the ISM, the cloud inhomogeneities can similarly have a profound effect on the structure of the SNR.

Recent observations of SNR of enhanced emission in the Balmer line filaments show evidence of cloud-shock interactions for Tycho (Braun, 1988). Velusamy (1987) finds evidence of the remnant cloud interaction in his radio observations of W28 and W44 taken at 327 MHz. These observations clearly show the distortion of the radio shell as the remnant begins to wrap around a dense cloud. The observations of the SNR IC443 by Braun and Strom (1986) show the later evolution of the cloud shock interacting with the outer layers of the cloud stripped off at high velocity.

Given the importance of the interaction of the supernova shocks with clouds for understanding the structure and the dynamics of the ISM as well as the potential importance of the interaction as a means of triggering new star formation, the problem has been studied both analytically and numerically over the past decade. Even when idealized as the interaction of a strong shock with a spherically symmetric cloud embedded in a less dense intercloud medium, the problem represents an extremely complex non-linear hydrodynamic flow encompassing a rich family of shock-shock interaction phenomena. The multi-dimensional nature of the evolution of the disrupted cloud is such as to make a detailed analytic calculation intractable. The first serious attempt to follow the interaction numerically was made by Woodward (1976), who used a combined Eulerian-Lagrangian approach to follow the interaction of the shock from a spiral density wave with a galactic cloud. These results showed the start of both Rayleigh-Taylor and Kelvin Helmholtz type instabilities; however, the calculation was not carried out far enough in time and lacked the spatial resolution to ascertain the final fate of the cloud. A subsequent attempt to investigate this problem by Nitman et al. (1982) used a flux-corrected transport approach and was very unresolved. Recently, Tenorio-Tagle and Rozyczka (1986) attempted to follow the evolution with a second order accurate hydrodynamic scheme, but again the calculation was under-resolved and clearly showed the effects of strong numerical diffusion at the interface of the cloud boundary and the intercloud medium. This made it

impossible to disentangle the mixing of cloud-intercloud matter due to physical instabilities from mixing due to numerical effects. All of the previous work on this important problem leave unanswered several questions of key importance: What is the ultimate fate of clouds that have been impacted by SNR shocks? What is the total momentum delivered to the cloud? How much mass is lost from the cloud? What are the mechanisms by which clouds are disrupted and to what extent does disruption take place? How does cloud morphology scale with cloud density, shock Mach number and cloud size? Is the cloud driven to gravitational instability or is the cloud destroyed? What is the effect of the interstellar magnetic field on the evolution? What are the observable consequences of the interaction?

We have recently found (Klein, Colella and McKee, 1989a) that highly complex shock-shock interactions play a major role in determining the morphology of the cloud. Instabilities and shear flow motions are crucial to track accurately. Small scale structure in the flow may contribute significant mass loss back to the ISM and must be well resolved. These physical phenomena place an enormous constraint on the capabilities of most conventional numerical methods for solution of the 2-D equations of hydrodynamics. Even high order accurate approaches such as PPM with fixed Eulerian grids would require at least  $10^6$  grid points to follow the evolution accurately enough to answer the questions posed above. Clearly, one has a great need to evolve 2-D hydrodynamics with a great enough accuracy to deal with physical constraints and at the same time do so economically in both storage and time.

### METHODOLOGY

To address these difficulties, we have used the local adaptive mesh refinement techniques with second order Godunov methods developed by Berger and Colella 1989 (cf. Klein, Colella, and McKee, 1989a). This first important problem will be the forerunner of a broad-based program we are developing to use adaptive mesh refinement to study astrophysical gas dynamics. We employ a second order finite difference solution of the 2-D Euler equations on a square grid in a cylindrically symmetric geometry. The numerical integration of the Euler equations is accomplished using an operator split version of a second order Godunov method (Colella and Woodward, 1984). The Godunov method conserves mass, momentum and total energy. We assume that the cloud and intercloud gas are both adiabatic, although we allow the cloud and intercloud medium to have different values of the adiabatic index  $\gamma$ . The resulting method is second order accurate in space and time, and captures shocks and other discontinuities with minimal numerical overshoot and dissipation.

From the point of view of being able to resolve detailed complex physical structures with reasonable amounts of supercomputer time and memory, the most important feature of our code is that it employs a dynamic regridding strategy known as local Adaptive Mesh Refinement (AMR) to dynamically refine the solution in regions of interest or excessive error. This is effected by placing a finer grid over the region in question with the grid spacing reduced by some even factor (typically 2) in each spatial dimension. The boundary of

the refined grid is always chosen to coincide with cell edges of the coarser grid. Multiple levels of grid refinement are possible with the maximum number of nested grids supplied as a parameter in the calculation. Typically our calculations employ two nested grids over the initial coarse grid. A level 3 grid has 256 cells for each cell in a level 1 grid. In our present work, we determine those regions which require refinement by estimating the local truncation error in the density and refining those regions where the error is greater than some initially specified amount. In addition, we require the maximum level of refinement in the neighborhood of all cells containing cloud material. Special care is taken to ensure the correct fluxes across boundaries between and fine grids. This dynamic adaptive gridding approach is a crucial factor in our ability to economically resolve important features in the cloud shock interaction.

### CLOUD SIZE SCALES

As the SNR expands through the ISM, it drives a shock into any cloud it encounters. Assuming that these are strong shocks, the pressure behind the blast wave and the pressure behind the transmitted cloud shock are comparable, and one finds that (McKee and Cowie, 1975)

$$v_s = (\rho_i / \rho_c)^{1/2} v_b, \quad (1)$$

where  $v_s$  and  $v_b$  are the cloud shock and blast wave velocities and  $\rho_c$  and  $\rho_i$  the initial cloud and intercloud densities, respectively. Following McKee (1988), we define characteristic timescales for the cloud-shock interaction. Let  $\chi \equiv \rho_c / \rho_i$  be the density contrast and assume that  $\chi \gg 1$ . Assume that the cloud is a sphere with radius  $a$  at a distance  $R_b$  from the supernova explosion. The blast wave in the Sedov-Taylor phase will expand as  $R_b \propto t^{2/5}$ , so the age of the SNR is,

$$t \equiv \frac{dR_b}{dt} = \frac{2}{5} \frac{R_b}{v_b}. \quad (2)$$

The blast wave in the intercloud medium crosses the cloud in a time

$$t_{ic} \equiv \frac{2a}{v_b}, \quad (3)$$

whereas the cloud shock crushes the cloud in a time

$$t_{cc} \equiv \frac{a}{v_s} = \frac{\chi^{1/2} a}{v_b}. \quad (4)$$

The cloud crushing time  $t_{cc}$  is of the order of the sound crossing time in the crushed cloud; it is also about the timescale for the growth of large scale Rayleigh-Taylor instabilities. Finally, the cloud accelerates up to the velocity of the intercloud gas in a characteristic drag time  $t_d$  defined by  $\rho_i v_b t_d = \rho_c a$ ,

or

$$t_d = \frac{\chi a}{v_b} = \chi^{1/2} t_{cc}. \quad (5)$$

In this paper, we will consider only clouds that can be characterized as "small", so that the SNR does not evolve significantly during the time for the cloud to be crushed:

$$t > t_{cc} \Rightarrow a < \frac{0.4R}{\chi^{1/2}}. \quad (6)$$

Indeed, we shall focus on the case in which the cloud is "very small", so that  $t \gg t_d$ , and  $a \ll 0.4R/\chi$ . In either case, we have  $a \ll R$  so that the blast wave may be treated as a planar shock. In the opposite limit of a shock interaction with a large cloud, the SNR blast wave will undergo substantial weakening over the time it takes to cross the cloud. We expect substantial disruption for the small clouds, but only impulsive effects for large clouds.

## CLOUD EVOLUTION

### a. Cloud Crushing

Since there are no intrinsic scales in the problem, it is parameterized by the Mach number of the SNR blast wave  $M$  and the density ratio  $\chi$ . Our calculations assumed 2-D axisymmetry for an inviscid fluid with no magnetic field. Two cases were considered for the cloud:  $\gamma = 1.1$  and  $\gamma = 5/3$ . The intercloud gas was assumed to have  $\gamma = 5/3$ . Several calculations have been made for Mach numbers in the range 10-1000 and density ratios 10-400.

It is useful to follow the morphological evolution of the cloud through several cloud crushing times to obtain a sense of the different stages of development. We present the time-development of the isodensity contours of the cloud for the case  $\gamma(\text{cloud}) = \gamma(\text{intercloud}) = 5/3$ ,  $\chi = 10$ ,  $M = 10$ . At  $t = 0.84 t_{cc}$  (Fig. 1), the transmitted shock is compressing the cloud from the front, secondary shocks have enveloped the sides of the cloud as the blast wave passes over the cloud, and a reflected bow shock moves upstream into the intercloud medium. The reflected shock becomes a standing bow shock and eventually a weak acoustic wave carrying away a small amount of energy from the supernova shock (Spitzer, 1982). At  $t = 1.05 t_{cc}$  (Fig. 2) the blast wave behind the cloud reflects off the axis giving rise to a Mach reflected shock back into the cloud. After  $t = 1.26 t_{cc}$  (Fig. 3), behind the cloud, a

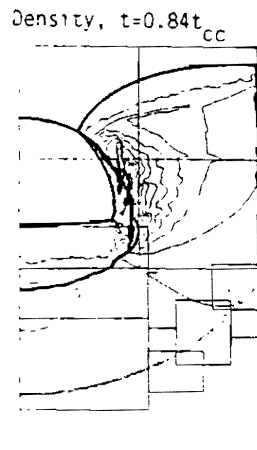


Figure 1

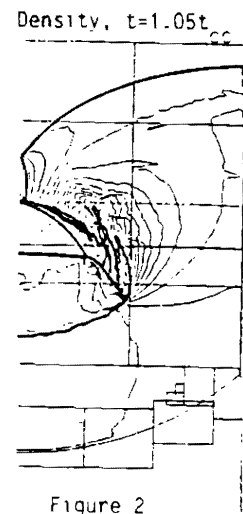


Figure 2

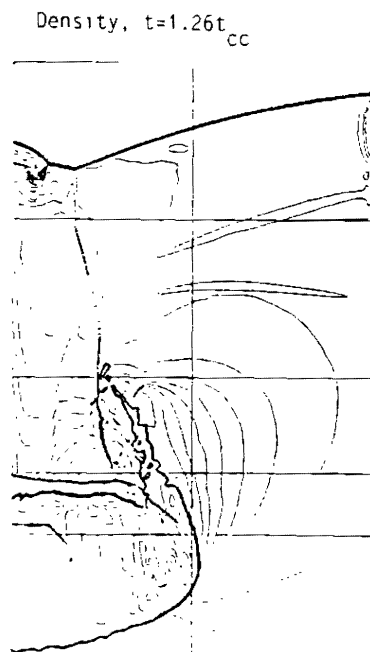


Figure 3

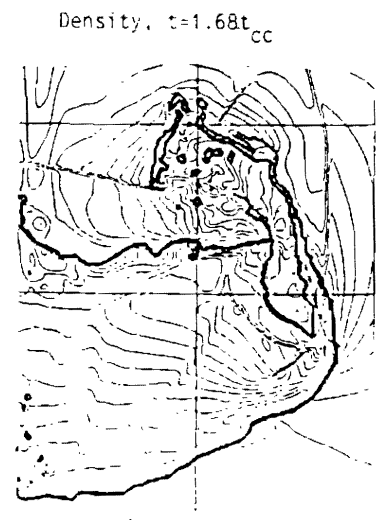


Figure 4

Isodensity contours of cloud and intercloud matter at different times.



Figure 2

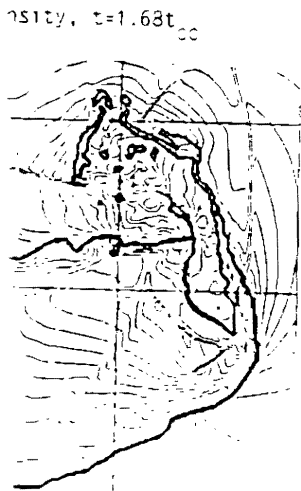


Figure 4

ferent times.

double Mach reflection with the appearance of two triple point interactions occurs. This classic oblique shock interaction (Hornung, 1986; Glaz et al. 1985) shows evidence of a strong supersonic vortex ring far behind the cloud. The vortex ring may have interesting observational consequences for SNRs (see below), but plays no role in the continued dynamical evolution of the cloud. The reflected shock and the transmitted shock undergo a strong interaction at  $t=1.68t_{cc}$  (Fig. 4) resulting in a initial flattening of the cloud. We also note the beginning of a strong shear flow. Substantial flattening of the cloud is observed at  $t=2.1t_{cc}$  from the strong shocks which have squeezed it like a vise. The pressure maximum on the nose of the cloud exceeds the pressure minimum on the sides and the cloud begins to expand laterally (Fig. 5). We note the growth of Richtmyer-Meshkov instabilities (Richtmyer, 1960) on the cloud nose which grow more slowly than the classic Rayleigh Taylor modes. At  $t=2.5t_{cc}$ , we see evidence of Kelvin Helmholtz instabilities, on the sides of the cloud; weak shocks still residing in the cloud interior dissipate their energy (Fig. 6).

#### b. Shear Flow and Vortex Production

At  $3.78t_{cc}$  a prominent shear layer exists due to the motion of the cloud through the ICM. The shear produces copious vortex rings along the shear flow layer and leads to substantial Kelvin-Helmholtz instabilities which break up the arms (Fig. 7). The cloud consists of a distorted unstable axially flattened core component and a severely disrupted halo of cloud material. Over 70% of the original cloud mass is in small fragments which, in the absence of cooling, should merge with the intercloud medium. The unstable break up is dominated by large scale differential shear. At  $t=9.7t_{cc}$ , the cloud is completely destroyed (Fig. 8) and consists of several thousand fragments. At  $4.2t_{cc}$  the strong supersonic vortex rings align along the shear flow layer produced in the dominant arm of cloud material that has been pulled from the main core of the cloud as well as along a second substantially fractured mass of cloud that has been fragmented from the arm. In Fig. 9 we show the associated flow field alongside of isodensity contours of the cloud and intercloud gas at  $t=4.2t_{cc}$ . It is clear that regions of strong circulation (high vorticity, numbered 1-5) are associated with positions along the shear flow layer where the cloud has undergone severe fragmentation. As vortex rings are formed in the shear layer and move away from the initial cloud are, the vortex rings are broken off. The process is called vortex shedding. It is suggestive of the possibility that the vorticity in the intercloud matter is acting to enhance the cloud break-up along the differential shear layer, thus acting as a mix-master aiding the development of the Kelvin-Helmholtz instabilities. This interesting possibility is worth further study.

To gain more insight into the development of the vortex rings we develop an equation for the time dependent change of the vorticity  $\omega \equiv \nabla \times u$  where  $u$  is the fluid velocity. The equation of motion with the inclusion of body forces  $F$  is

$$\frac{\partial u}{\partial t} + (u \cdot \nabla) u = \frac{-\nabla P}{\rho} + \frac{F}{\rho} \quad (7)$$

Density,  $t=2.1t_{cc}$



Figure 5

Density,  $t=2.5t_{cc}$



Figure 6

Density,  $t=3.78t_{cc}$

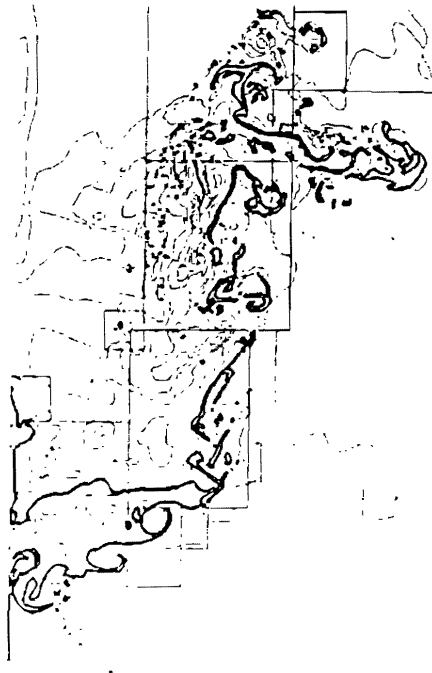


Figure 7

Density,  $t=9.7t_{cc}$

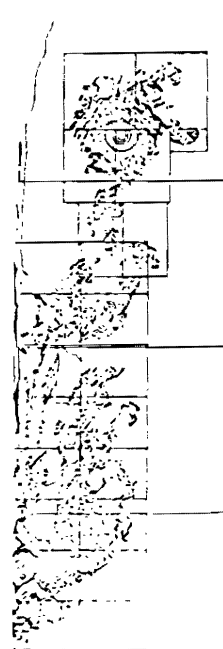


Figure 8

Figure 6  
y,  $t=2.5t_{cc}$



Figure 6

Figure 8  
y,  $t=9.7t_{cc}$

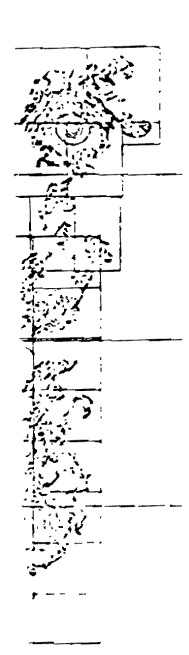


Figure 8

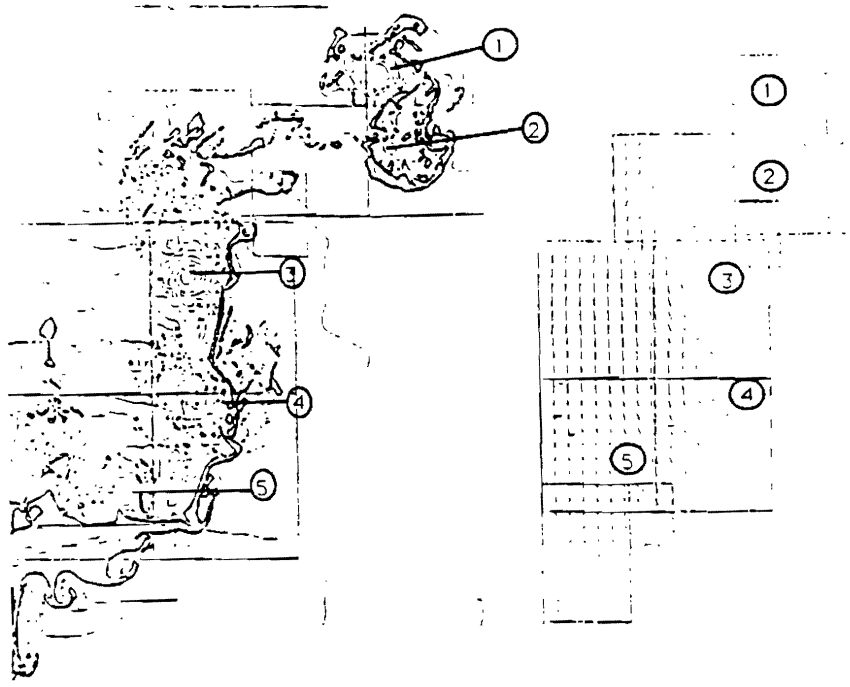


Figure 9 Isodensity contours (on left) at  $t=4.2t_{cc}$ , flow field (on right). Numbers are sites of vorticity maximums.

Using the vector identity

$$(\nabla \times \mathbf{u}) \times \mathbf{u} = (\mathbf{u} \cdot \nabla) \mathbf{u} - \frac{1}{2} \nabla(u^2) \quad (8)$$

we find

$$\frac{\partial \mathbf{u}}{\partial t} + \omega \times \mathbf{u} = \frac{-\nabla P}{\rho} + \frac{\mathbf{F}}{\rho} - \frac{1}{2} \nabla u^2 \quad (9)$$

Now taking the curl of each side and using the identity

$$\nabla \times (\omega \times \mathbf{u}) = \omega \nabla \cdot \mathbf{u} + (\mathbf{u} \cdot \nabla) \omega - \omega \cdot \nabla \mathbf{u}, \quad (10)$$

we derive the material derivative of the time rate of change of the vorticity

$$\frac{d\omega}{dt} = \omega \cdot \nabla \mathbf{u} - \omega \nabla \cdot \mathbf{u} - \frac{\nabla P \times \nabla \rho}{\rho^2} + \nabla \times (\mathbf{F}/\rho). \quad (11)$$

We see that the vorticity depends upon four processes. The first term is a shear term which represents vortex-tube stretching. The second term represents the effects of compression: If the vorticity filaments bunch together the magnitude of the vorticity component increases in the direction of the vortex filament. If these were the only two processes, then the circulation  $\int \omega \cdot d\mathbf{A} = \oint \mathbf{v} \cdot d\boldsymbol{\ell}$  would be conserved. The next term is a baroclinic term which is the major source of vorticity in the cloud-shock interaction. The shock impinges on the cloud obliquely and produces surfaces of constant pressure that are not coincident with surfaces of constant density at the interface of the cloud and intercloud matter. This gives a non-zero cross product of gradients. The vorticity in the ICM is greater than that in the cloud because of the higher velocities in the lower density material. Our calculations show that most of the vorticity remains concentrated near the cloud boundary, where it originated. The fourth term is important if the fluid is viscous. If the force  $\mathbf{F}/\rho$  is frictional, it can be represented as  $\mathbf{F}/\rho = \nu \nabla^2 \mathbf{u}$  where  $\nu$  is the viscosity; then  $\nabla \times (\mathbf{F}/\rho) \sim \nu \nabla^2 \omega$ . This represents the diffusion of vorticity from regions of high to low concentration. It is proportional to the amount of numerical viscosity in the finite difference approximations. Given the importance of vorticity as a possible observational diagnostic of the remnant cloud interaction as well as its possible role in the cloud fragmentation, it is of great importance to demonstrate that numerical viscosity does not play a role in determining the amount of vorticity production. We have computed the time evolution of the cloud for four increasingly resolved initial grids, doubling the

number of cells in both  $\Delta r$  and  $\Delta z$  with each increase in resolution. We have shown that the time evolution of the vorticity for even the coarsest mesh ( $\Delta x = .08$  in code units, corresponding to about half of the initial cloud radius) tracks to a remarkable degree of accuracy the vorticity of the finest resolution, which is equivalent to a  $7 \times 10^6$  zone calculation for a fixed grid method. This clearly establishes that numerical viscosity, which is proportional to grid resolution, does not affect the production of vorticity for the adaptive grid techniques we are using. This type of calculation is a powerful check on the conservation of vorticity.

Let us consider the characterization of the evolution of the interstellar cloud in more detail. In Table 1, we display the results of adiabatic calculations for three models in which  $\gamma = 5/3$  in both the cloud and ICM. The calculations are done for two models ( $M=10$  and  $100$ ) for density contrast  $\chi = 10$  and one model ( $M=100$ ) for density contrast 100. The first entry in the table is the time normalized to the intercloud crossing time. The second entry gives the time normalized to the cloud crushing time and the drag time,  $t_d = \chi^{1/2} t_{cc}$ . The next column is the sound speed behind the cloud shock normalized to the blast wave velocity. The shocked intercloud gas moves at a velocity  $(3/4) v_B$  relative to the cloud for  $\gamma = 5/3$ , so the next entry measures the ratio of the current cloud/intercloud relative velocity  $\Delta v$  to its initial value; in the frame of the shocked intercloud gas, this is a measure of cloud deceleration. The next column is a characterization of the cloud's aspect ratio in the radial and axial direction weighted by its half mass distribution. Here  $r_{1/2}$  is the radial half-mass distance and  $Z_{1/2}$  is the axial half-mass distance. The last column gives the radial  $\dot{r}_{1/2}$  and axial  $\dot{Z}_{1/2}$  expansion velocities of the cloud. These velocities are computed by using the half mass distance distributions at the two final times in the calculation.

Several conclusions can be drawn from these results. Comparing the results at the same normalized "final" time  $t = 4.2 t_{cc}$  for clouds of the same density  $\chi = 10$ , but subjected to blast waves of different Mach number, 10 and 100, we note that both clouds have decelerated to about 0.15 of their initial velocities. Thus, these clouds have almost stopped, leading to a small pressure differential between the front of the cloud surface and the sides so that there is little force driving further radial expansion; hence the clouds have a radial expansion velocity  $\dot{r}_{1/2} \approx 0$ . The strong shear flow in the cloud is still dominant, however, and both clouds are supersonically shearing apart at about the same axial expansion velocity  $\dot{Z}_{1/2}$  of 3 times the cloud velocity. The physical extent of the stretching in both the radial and axial direction

$$\frac{r_{1/2}(t)}{r_{1/2}(0)}, \frac{Z_{1/2}(t)}{Z_{1/2}(0)}$$

is essentially the same for the two cases. The remarkable agreement of these features of the clouds and their similar morphological structure leads one to suspect that the cloud evolution may scale similarly with the Mach number of the SNR shock. This Mach scaling can be clearly seen if we scale the time, velocity and pressure as  $t = t/M$ ,  $v = vM$  and  $P = PM$ . Substituting these scaled quantities into the Euler equations, we find that Euler equations are

(8)

(9)

(10)

the vorticity

(11)

The first term is  
The second term  
its bunch together  
e direction of the  
en the circulation  
a baroclinic term  
interaction. The  
faces of constant  
nt density at the  
a non-zero cross  
n that in the cloud  
. Our calculations  
e cloud boundary,  
; is viscous. If the  
 $\partial u$  where  $v$  is the  
usion of vorticity  
l to the amount of  
ions. Given the  
tic of the remnant  
mentation, it is of  
s not play a role in  
omputed the time  
rids, doubling the

invariant under this transformation. Thus, we find that for fixed  $\gamma$  and density contrast  $\chi$ , the morphological evolution is a function of  $t/t_{cc}$  only, in the limit of large  $M$ .

Clouds with greater density contrasts  $\chi$  show greater expansion in both the radial and axial directions, as shown both by the results in Table 1 and by Figures 10 and 11, which portray the state of a shocked cloud with  $\chi = 100$  at  $4 t_{cc}$  and  $\chi = 400$  at  $2 t_{cc}$ . This follows from the fact that the characteristic expansion time for the cloud is the sound crossing time (which, as remarked above, is about  $t_{cc}$ ), whereas the time for the cloud to decelerate is the drag time  $t_d = \chi^{1/2} t_{cc}$ . The lateral expansion of the cloud is due to the lower pressure on the sides of the cloud caused by the Venturi effect (Nittman et al. 1982). This pressure difference decays on the drag time; by the time shown in Figure 11, this expansion has stopped. At  $t = 4 t_{cc}$ , the axial expansion velocity is a substantial fraction of  $v_b$  for both  $\chi = 10$  and  $\chi = 100$ ; since  $t_{cc}$  is larger for  $\chi = 100$ , the length of the cloud is greater in this case. We expect the axial expansion of the cloud to stop within a few drag times. This has been verified for the  $\chi = 10$  case, but not the  $\chi = 100$  case.

### c. Cloud Fragmentation

At late times (several  $t_{cc}$ ) the cloud is rendered to a turbulent flow with several fragments reduced to a foam on the scale of grid resolution. It is of great interest to follow the mass loss of the cloud as it fragments, and to understand how the fragmentation scales with varying cloud density. In Fig. 12, we show the mass of the cloud core as a function of time for clouds with density contrasts  $\chi=10,100,400$ . The cloud core is defined to be the most massive cloud fragment. The mass loss vs time has been fitted with an exponential to determine the fragmentation time  $t_f$ , defined as the time for each cloud to be left with  $1/e$  of its original mass. We find for  $\chi=10$  that the cloud fragments initially into two roughly equal mass fragments. The mass fragments then begin a series of further fragmentation stages into smaller pieces due to combined Rayleigh Taylor and Kelvin Helmholtz instabilities. We have developed an algorithm that performs pattern recognition of fragments on our hierarchical grid structure and sorts their masses to produce a mass spectrum for fragmentation. Fig. 13 shows the fragment mass plotted against the mass in each bin for the  $\chi=10, M=10$  case at  $t=3.78 t_{cc}$ . We note that the cloud has broken into two fragments of essentially the same mass comprising about 78% of the mass of initial cloud, two additional fragments comprising ~9% of the initial mass and ~580 fragments accounting for the remaining 12% of the initial mass. In Fig. 14 we blow-up the low mass end of the spectrum (12% of the initial mass) where we see the distribution of the more massive of these low mass fragments. Mass fragmentation spectra such as these can provide a distinct "fingerprint" of the way in which a cloud undergoes fragmentation and are a powerful tool to establish scaling properties for different clouds with varying conditions. We are in the process of determining which aspects of this fragmentation are physical and which are affected by numerical resolution. In Fig. 8 we show isodensity contours of the cloud at  $t=9.67 t_{cc}$  where the cloud is completely destroyed. The final fate

ly and density  
ly, in the limit

ansion in both  
Table 1 and by  
with  $\chi = 100$  at  
characteristic  
s, as remarked  
ate is the drag  
to the lower  
Nittman et al.  
time shown in  
al expansion  
0; since  $t_{cc}$  is  
e. We expect  
es. This has

ent flow with  
tion. It is of  
ents, and to  
density. In  
ie for clouds  
ed to be the  
fitted with a  
ime for each  
at the cloud

The mass  
into smaller  
instabilities.  
ognition of  
s to produce  
mass plotted  
 $t_c$ . We note  
same mass  
l fragments  
ting for the  
w mass end  
ution of the  
pectra such  
ch a cloud  
g properties  
process of  
which are  
ontours of  
e final fate



Figure 10 Isodensity contours for  $\chi=100$ ,  $M=100$  at  $t=4.0 t_{cc}$

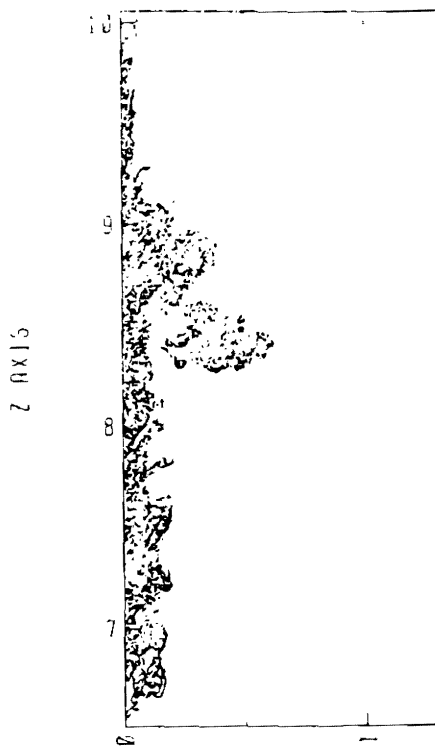


Figure 11 Isodensity contours for  $\chi=400$ ,  $M=100$  at  $t=2.0 t_{cc}$ . Note morphology of cloud consisting of a dense "head" followed by a trail of several thousand fragments with an aspect ratio of 20 to 1.

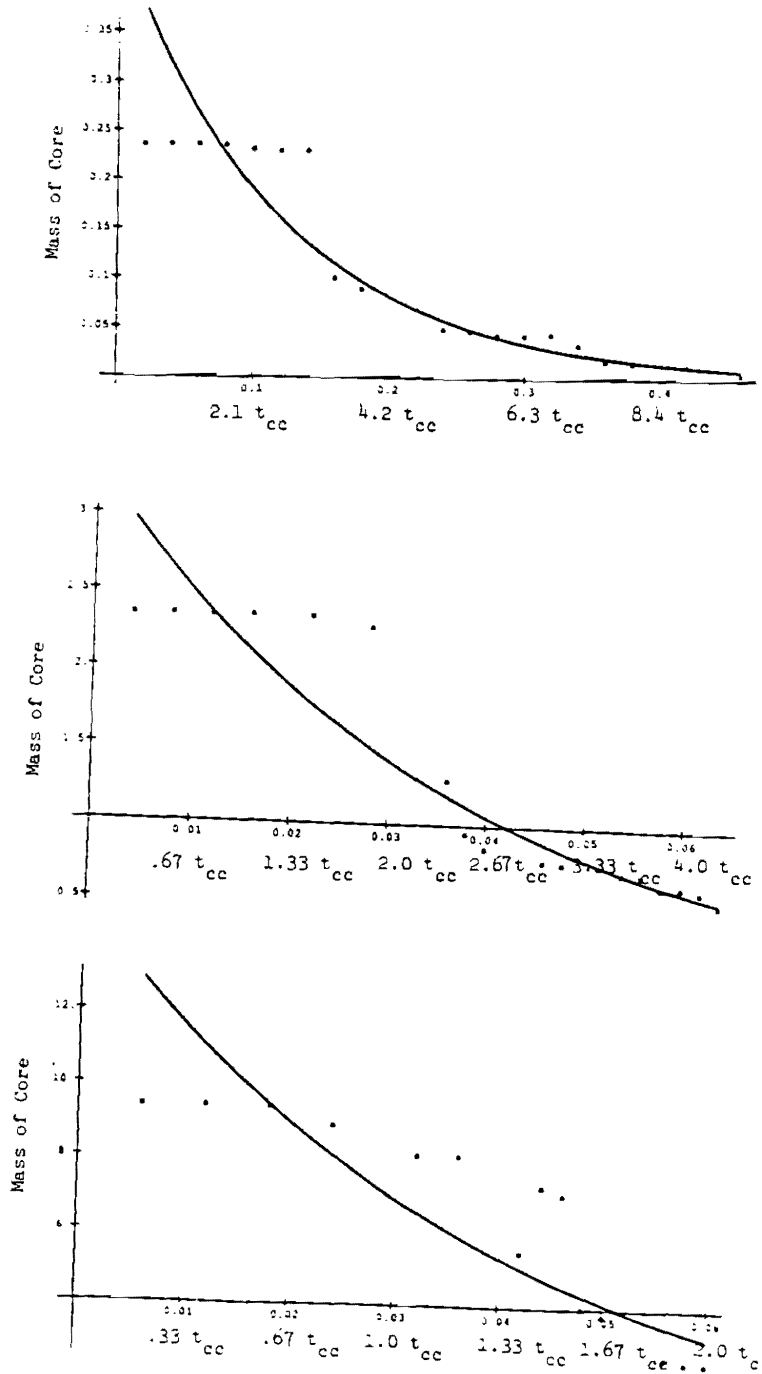


Figure 12 Core mass vs time for  $\chi=10, 100, 400$

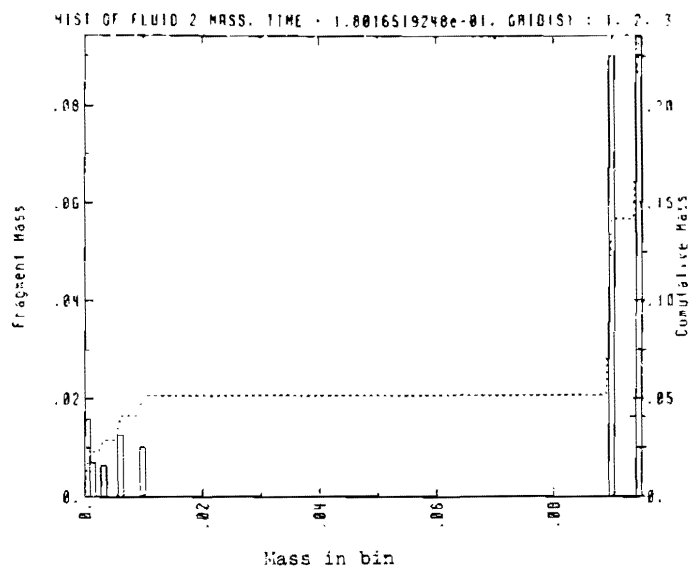


Figure 13 Fragment mass vs mass in bin for  $\chi=10$ ,  $M=10$  at  $t=3.78 t_{cc}$

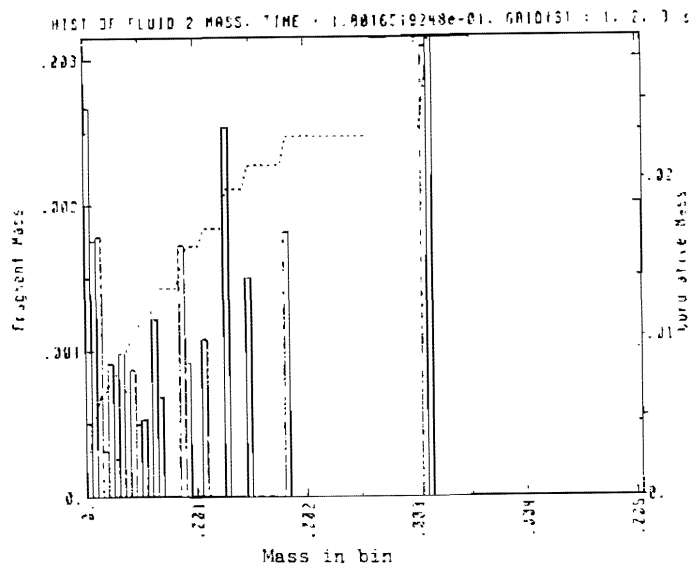


Figure 14 Fragment mass vs mass in bin for  $\chi=10$ ,  $M=10$  at  $t=3.78 t_{cc}$  at low mass end of the fragmentation spectrum.

0.06  $t_{cc}$

of this cloud consists of a quasi-static halo of fragments of which 50% of the mass resides in an axially elongated distribution stretched out 5-6 times its initial shape, and the rest of the mass resides in a multitude of fragments much less dispersed.

For clouds with  $\chi \gg 10$ , the stripping process proceeds differently. For  $\chi=400$ , the cloud fragments gradually, with a continuous erosion by loss of small fragments (cf. Fig. 11 and Fig. 12). Since small fragments rapidly become comoving with the intercloud medium whereas the cloud core decelerates gradually, small fragments trail far behind the massive cloud core until the core itself is destroyed by Kelvin-Helmholtz instabilities as it drags through the intercloud medium. In Fig. 11 the cloud core mass at  $t = 2t_{cc}$  is 26% of the original cloud and we see that the cloud has the distinct morphology of a dense cloud core trailed by a multitude of fragments in a narrow tail.

Our results show that clouds are fragmented in a time  $t_f \sim (1.5 - 4) t_{cc}$  as  $\chi$  ranges from 400 to 10; recall that  $t_{cc}$  is of order the Rayleigh Taylor timescale. The numerical coefficient is smaller for the higher density contrasts, presumably because the relative velocity of the cloud remains greater.

This conclusion is consistent with that of Nittman et al. (1982), who concluded that the cloud would be destroyed in a time  $\sim 3 t_{cc}$  due to the combined effect of lateral expansion and strong fluid rotation behind the cloud. Because of the increase in the cross section of the cloud due to the lateral expansion, the time for the fragmented cloud to accelerate up to a velocity comparable to that of the shocked ICM is several times less than the initial drag time  $t_D = \chi a/v_b$ . Thus for  $\chi \lesssim 10^2$ , the fragmentation time and the acceleration time are comparable; on this point, our conclusion differs from that of Nittman et al. In an analytic study of the related problem of the stripping of gas from a galaxy moving through an intracluster medium, Nulsen (1982) concluded that the stripping time is of the order of the drag time  $t_d$ ; in the absence of gravitational effects (which he found to be generally small), our results indicate that stripping will occur substantially more rapidly.

We have performed calculations for several similar models for  $\gamma=1.1$  in the cloud. This softer equation-of-state is more representative of clouds that are radiative, although it should be pointed out that truly radiative clouds can get rid of their stored energy efficiently, and we would expect substantially more shock compression than the models considered here. We note that these "radiative" clouds move substantially more rapidly than their  $\gamma=1.67$  counterparts. These clouds are significantly more radially compressed, and thus experience far less drag than the  $\gamma=1.67$  clouds. This can again be understood by consideration of the sound speed in these clouds. We find that the scaling of sound speed  $c_c$  with  $\gamma$  is such that  $c_c(\gamma=1.1) \ll c_c(\gamma=5/3)$ , so that these "radiative" clouds expand laterally more slowly. We note that the high density "radiative" cloud is still experiencing large supersonic axial shearing. As with the previous  $\gamma=5/3$  models Mach scaling appears to be established.

### OBSERVATIONAL CONSEQUENCES

An outcome of these calculations that may be potentially very important for observations of SNR is the discovery of the copious production of vortex rings distributed along the strong shear flow layer (Fig. 9). Approximating the rotation of these vortices by rigid body rotation, we can relate the vorticity  $\omega$  in an individual vortex ring to the pressure differential across the vortex  $\Delta P$ , and we find that  $\omega = (8\Delta P/\rho)^{1/2}/r$ . This appears to be an excellent approximation when compared to our detailed calculations. Those rings with large aspect ratio may be subject to non-axisymmetric instabilities and break up into yet smaller vortex structures (Saffman and Baker, 1979). "Fat" rings, with small aspect ratio, are likely to remain intact. Recent high resolution radio observations of the Cas A SNR (Tuffs, 1986) have revealed several hundred intense compact radio emission peaks distributed throughout the remnant. We have demonstrated that strong shear flows associated with shock-cloud interactions result in the production of many supersonic vortex rings. These vortex rings can be expected to wind up ambient magnetic fields present in the interstellar clouds until equipartition between the energy in the field and the vortex is achieved. It is quite possible that the resulting intense wound up magnetic field and the associated betatron acceleration could account for the synchrotron emission of electrons, thus explaining the observations in Cas A. Equipartition magnetic fields are often invoked in astrophysics to explain non-thermal emission; our results suggest that the fields may indeed reach equipartition, but only in a small fraction of the volume. Chevalier (1976) postulated the presence of turbulent vortices, acting as magnetic scattering centers in SNRs to explain particle acceleration by a second-order Fermi mechanism. We conjecture that the radio hot spots may indeed be indirect observational evidence of the presence of vortex rings produced behind the shocked clouds. The vortex rings would have low density and pressure at the center, thus appearing weak in optical, UV and x-ray emission.

Finally, the cloud morphology itself is an important signature. The clouds can be expected to be elongated structures with aspect ratios  $\sim 5-6$ , with multitudes of fragments trailing behind the cloud core. A possible example of this has been observed by Braun and Strom (1986) in IC443.

### CONCLUSIONS

We have performed second order accurate, high resolution local adaptive mesh refinement calculations of the interaction of a supernova shock with interstellar clouds. These extremely powerful hydrodynamic techniques have enabled us to calculate exceedingly complex flows much more rapidly, much more accurately, and much further in time than previous work with standard fixed grid hydrodynamics. We have followed the evolution of interstellar clouds well into the regime of fragmentation. Our calculations have demonstrated high accuracy with 80,000 grid cells that would only be achievable with fixed grid high order accurate hydrodynamic schemes with  $>1,000,000$  grid cells. We find:

- 1) Small non-radiative interstellar clouds are efficiently destroyed in a few cloud crushing times times by combined Rayleigh-Taylor and Kelvin Helmholtz instabilities dominated by large scale shear flow. Clouds that have the same density but are enveloped by strong shocks of differing Mach number exhibit scaling behavior in their morphological evolution.
- 2) Small clouds are highly fragmented by non-radiative shocks. Cloud fragments will most likely eventually feed their mass back into the ISM by thermal evaporation.
- 3) Small adiabatic clouds fragment to such an extent that it is unlikely that fragments large enough to become gravitationally unstable and form stars will survive. The cloud destruction proceeds more rapidly than the free fall time.
- 4) Clouds evolve toward a elongated structures with aspect ratios of five to six, consisting of multitudes of fragments.
- 5) Our calculations indicate the copious production of supersonic vortex rings. These vortex rings may be effective in winding up the ambient magnetic field in clouds, increasing the magnetic field strength and enhancing the synchrotron emission of cosmic ray electrons. This could explain the recent observations of numerous compact radio hot spots in Cas A.

In the future, we shall use adaptive mesh refinement hydrodynamic techniques to investigate a broad range of astrophysical gas dynamical phenomena.

#### ACKNOWLEDGEMENTS:

The calculations presented in this paper were performed on the XMP416 and YMP832 at the Lawrence Livermore National Laboratory. This work was performed under the Auspices of the U.S. DOE by LLNL under Contract W-7405-Eng-48, supported in part by the Applied Mathematical Sciences Program of the office of energy research, and was also performed in part under the auspices of a special NASA astrophysics theory program which supports a joint Center for Star Formation Studies at NASA Ames Research Center, University of California, Berkeley, and University of California, Santa Cruz. The work of CFM is supported by NSF grant AST 86-15177.